Eur. Phys. J. B **27**, 409–415 (2002)
DOI: 10.1140/epjb/e2002-00172-3

THE EUROPEAN PHYSICAL JOURNAL B

Magnetic dipole and electric quadrupole responses of elliptic quantum dots in magnetic fields

E. Lipparini[1], Ll. Serra[2,a], and A. Puente[2]

[1] Dipartimento di Fisica, Università di Trento, and INFM sezione di Trento, 38050 Povo, Italy
[2] Departament de Física, Universitat de les Illes Balears, 07071 Palma de Mallorca, Spain

Received 29 November 2001
Published online 6 June 2002 –

Abstract. The magnetic dipole (M1) and electric quadupole (E2) responses of two-dimensional quantum dots with an elliptic shape are theoretically investigated as a function of the dot deformation and applied static magnetic field. Neglecting the electron-electron interaction we obtain analytical results which indicate the existence of four characteristic modes, with different B-dispersion of their energies and associated strengths. Interaction effects are numerically studied within the time-dependent local-spin-density and Hartree approximations, assessing the validity of the non-interacting picture.

PACS. 73. Electronic structure and electrical properties of surfaces, interfaces, thin films, and low-dimensional structures – 73.20.Mf Collective excitations (including excitons, polarons, plasmons and other charge-density excitations)

1 Introduction

The electric dipole (E1) response of quantum dots has deserved much attention in recent years, mainly motivated by the measurements of far-infrared absorption in these systems [1,2]. The manifestation of the so called *magnetoplasmons* in a perpendicularly applied magnetic field constitutes an example of collective oscillation in finite Fermi systems, physically analogous to those existing in metal clusters, atoms or nuclei. In parabolically confined dots magnetoplasmons are understood as rigid motions of the electronic center of mass, a result that stems from the generalized Kohn's theorem [3–7]. However, deviations from parabolicity, such as angular deformations or non-quadratic radial behaviour, may result in more complicated absorption patterns which are currently being much investigated [8–11].

The understanding of other excitation modes of quantum dots are also essential for a proper characterization of these systems. Techniques based on resonant inelastic light scattering have already proved extremely useful to this purpose [12–15]. In fact, using polarization selection rules they permit to disentangle charge-density from spin-density and single-particle excitations, as well as to discern different multipolarity peaks in each channel. The momentum transfer and magnetic field dependence of the different excitations of a single sample have been recently reported using this technique [15]. It is worth to mention that theoretical analysis of the Raman spectra in circularly symmetric quantum dots have been presented in references [16–18].

In a recent work [19] Austing *et al.* have reported the fabrication of vertical quantum dots with assumed elliptical shapes, and the measurement of their addition energy spectra. In elliptical quantum dots the existence of orbital-current modes and their relationship with the quadrupole (E2) and magnetic dipole (M1) responses were analysed by us in reference [20]. A characteristic low energy mode, depending on deformation and with a conspicuous signal in the M1 channel was found in reference [20], while the relevance of orbital excitations in the build-up of the electronic moment of inertia was discussed in reference [21].

In this paper we shall focus on the magnetic field dependence of the orbital and quadrupole modes of elliptical dots, ranging from circular to well elongated appearances. A strictly two dimensional motion as well as the effective-mass-Hamiltonian approximation will be assumed to characterize the electronic states. This is considered to be a reasonable approach to the low energy states of quantum dots embedded in GaAs [19]. Understanding the M1 and E2 responses of deformed dots constitutes a necessary step towards the description of Raman scattering in symmetry unrestricted nanostructures. It will be shown that four excitation modes with B-dependent energies and strengths characterize both M1 and E2 responses. This result follows from analytical calculations in the so-called non-interacting deformed-harmonic-oscillator (NIDHO) model, as well as for interacting electrons in the local-spin-density (LSDA) and

[a] e-mail: dfslsc4@clust.uib.es

Hartree approximations. Therefore, it constitutes a robust picture against interactions in a somewhat similar way as Kohn's modes are.

This paper is organized as follows: Section 2 is devoted to the NIDHO model for M1 and E2 responses; in Section 3 we present the time-dependent LSDA results for the same channels and compare also with the Hartree model which neglects exchange and correlation effects; finally, Section 4 presents the conclusions.

2 The NIDHO model

2.1 The analytic solution of the ground state

We consider a system of non-interacting electrons, confined to the xy plane by an anisotropic parabola [22]

$$v^{(\mathrm{conf})}(x,y) = \frac{1}{2}\left(\omega_x^2 x^2 + \omega_y^2 y^2\right). \tag{1}$$

This potential, used in reference [19] to analyze the experiments on addition energies of vertical dots, will describe varying elliptical shapes, depending on the parabolas in x and y directions. In the following we shall fix the mean value $\omega_0 = (\omega_x + \omega_y)/2$ and label the dot deformation with the parameter $\delta = \omega_y/\omega_x$ (ranging from 0 to 1). Taking into account a uniform magnetic field $\mathbf{B} = B\mathbf{e}_z$, the system Hamiltonian reads

$$H = \sum_{i=1}^{N}\left[\frac{1}{2}\left(\mathbf{p_i} + \gamma\mathbf{A}(\mathbf{r}_i)\right)^2 + v^{(\mathrm{conf})}(\mathbf{r}_i)\right] + \frac{1}{2}g^* m^* \gamma B S_z, \tag{2}$$

where $\gamma = e/c$ (we assume Gaussian magnetic fields) and within the symmetric gauge $\mathbf{A}(\mathbf{r}) = B/2(-y, x)$. The last piece is the Zeeman term, depending on the total spin S_z and the effective gyromagnetic factor g^* [23]. Obviously this is a one-electron picture, in which the relevant one-electron Hamiltonian is $h = h_{xy} + \frac{1}{2}g^* m^* \gamma B s_z$. Because of the magnetic field, the spatial part h_{xy} deviates from a simple harmonic oscillator problem. Namely

$$h_{xy} = \frac{1}{2}\left(p_x^2 + p_y^2\right) + \frac{\omega_c}{2}\left(xp_y - yp_x\right) + \frac{1}{2}\left(\tilde{\omega}_x^2 x^2 + \tilde{\omega}_y^2 y^2\right), \tag{3}$$

with $\tilde{\omega}_x^2 = \omega_x^2 + \frac{1}{4}\omega_c^2$ and $\tilde{\omega}_y^2 = \omega_y^2 + \frac{1}{4}\omega_c^2$ the new parabola coefficients, given in terms of the cyclotron frequency $\omega_c = eB/c$.

The nontrivial problem posed by equation (3) has been elegantly solved in an analytical way, by Dippel *et al.* [24] and Madhav and Chakraborty [25] in the context of atomic physics and quantum dots, respectively. In the following, we will refer to the derivation by Dippel *et al.* They introduce a similarity transformation to a new Hamiltonian $h_3 = U^{-1}h_{xy}U$, where $U = \mathrm{e}^{\mathrm{i}\alpha xy}\mathrm{e}^{\mathrm{i}\beta p_x p_y}$. The parameters α and β are chosen in order to obtain two decoupled oscillators in the x and y directions

$$h_3 = \frac{p_x^2}{2M_1} + \frac{p_y^2}{2M_2} + \frac{M_1}{2}\omega_1^2 x^2 + \frac{M_2}{2}\omega_2^2 y^2. \tag{4}$$

The reader is addressed to reference [24] for the detailed expressions of α, β, M_1, M_2, ω_1 and ω_2 in terms of the original Hamiltonian parameters.

Most importantly, we can now express the eigenstates of h_{xy} in terms of those of h_3. The latter are simply products of one-dimensional oscillator functions with a given number of quanta, *i.e.*,

$$h_3\Phi_{n_1n_2}(x,y) = E_{n_1n_2}\Phi_{n_1n_2}(x,y)$$
$$\Phi_{n_1n_2}(x,y) = \phi_{n_1}(x)\phi_{n_2}(y), \tag{5}$$

while the eigenstates of h_{xy} are given by

$$h_{xy}\Psi_{n_1n_2}(x,y) = E_{n_1n_2}\Psi_{n_1n_2}(x,y),$$
$$\Psi_{n_1n_2}(x,y) = U\,\Phi_{n_1n_2}(x,y). \tag{6}$$

Notice that the energy eigenvalues of h_{xy} coincide with those of h_3 and that they are

$$E_{n_1n_2} = \left(n_1 + \frac{1}{2}\right)\omega_1 + \left(n_2 + \frac{1}{2}\right)\omega_2. \tag{7}$$

Having the one-electron states it is then a simple matter to obtain the N electron ground state of the NIDHO model just by filling the N lower energy orbitals.

2.2 M1 response

The excitations within the NIDHO model will correspond to independent particle-hole (ph) transitions in the level scheme of the ground state. Taking the orbital angular momentum ℓ_z as excitation operator the M1 strength function will be given by

$$S_{\mathrm{M1}}(\omega) = \sum_{hp} f_h(1-f_p)\left|\langle n_1^h n_2^h|U^{-1}\ell_z U|n_1^p n_2^p\rangle\right|^2 \times\delta(E_p - E_h - \omega), \tag{8}$$

where we have denoted the electron states $\Phi_{n_1n_2}$ as $|n_1n_2\rangle$ and the occupation numbers are given by the f factors.

To evaluate the matrix element in equation (8) we first need to obtain the transformed operator. This can be accomplished by using the Baker-Haussdorf lemma for unitary transformations [26], which introduces a nested commutators expansion. A straightforward calculation yields

$$U^{-1}\ell_z U = (1-2\alpha\beta)\ell_z + \beta(1-\alpha\beta)(p_x^2 - p_y^2) + \alpha(x^2 - y^2). \tag{9}$$

From equations (8) and (9) it emerges that there are only four allowed transition energies: $\omega_{11} = 2\omega_1$, $\omega_{22} = 2\omega_2$,

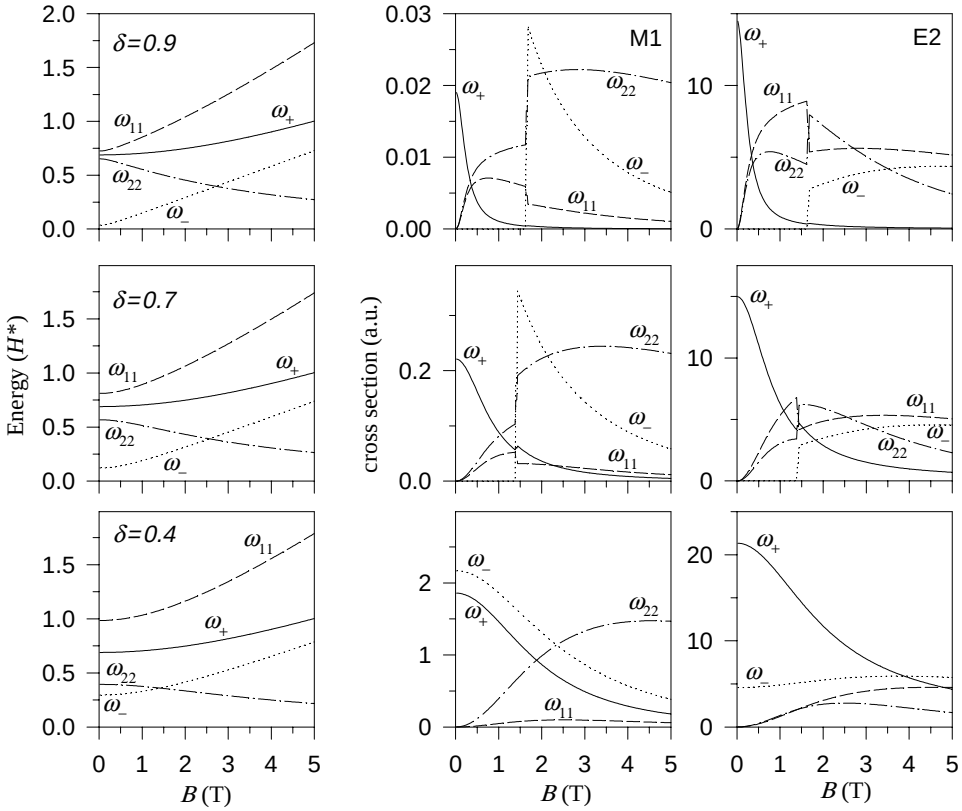

Fig. 1. Results within the NIDHO model for a $N = 6$ electron dot with $\omega_0 = 0.35$ H*. Left panels display the mode energies in H* while central and right ones show the M1 and E2 absorption cross sections $\omega S(\omega)$ as a function of the magnetic field. Each row corresponds to a different dot deformation.

$\omega_+ = \omega_1 + \omega_2$ and $\omega_- = |\omega_1 - \omega_2|$ whose M1 strengths are

$$S_{\rm M1}(\omega_{11}) = \frac{(\alpha - \beta(1-\alpha\beta)M_1^2\omega_1^2)^2}{4M_1^2\omega_1^2} \times \sum_{\text{occ. levels}} (1 - f_{n_1+2\,n_2})(n_1+1)(n_1+2)$$

$$S_{\rm M1}(\omega_{22}) = \frac{(\alpha - \beta(1-\alpha\beta)M_2^2\omega_2^2)^2}{4M_2^2\omega_2^2} \times \sum_{\text{occ. levels}} (1 - f_{n_1\,n_2+2})(n_2+1)(n_2+2)$$

$$S_{\rm M1}(\omega_+) = \frac{(1-2\alpha\beta)^2}{4M_1M_2\omega_1\omega_2}(M_2\omega_2 - M_1\omega_1)^2 \times \sum_{\text{occ. levels}} (1 - f_{n_1+1\,n_2+1})(n_1+1)(n_2+1)$$

$$S_{\rm M1}(\omega_-) = \frac{(1-2\alpha\beta)^2}{4M_1M_2\omega_1\omega_2}(M_2\omega_2 + M_1\omega_1)^2 \times \sum_{\text{occ. levels}} (1 - f_{n_1+1\,n_2-1})(n_1+1)n_2. \quad (10)$$

Result (10) provides a clear interpretation of the different modes: ω_{11} corresponds to the absorption of two x-oscillator quanta, ω_{22} absorbs two y quanta while ω_+ takes one quantum in each oscillator. By contrast, ω_- is associated with the absorption of one x quantum accompanied by the emission of a y quantum. We remind the reader that our convention ($\omega_y \leq \omega_x$) renders the absorption of a y quantum accompanied by the emission of an x quantum energetically forbidden.

Figure 1 depicts the absorption energies and associated intensities $\omega S(\omega)$ as a function of the magnetic field for different deformations in a quantum dot with $N = 6$ electrons and $\omega_0 = 0.35$ H*. For $\delta \geq 0.7$, when the system is just slightly deformed ($\delta = 1$ corresponds to the circular case), only the ω_+ mode is active at low B's. As the magnetic field is increased, very rapidly the ω_{11} and ω_{22} modes gain strength and disperse in energy. Eventually, for very large magnetic fields ω_{22} becomes the lowest energy mode and carries most of the strength.

The ω_- mode deserves a special discussion. Deformed dots at low deformation and magnetic field are characterized by the same oscillator occupancy numbers of the corresponding circular limit. In the case of magic number dots ($N = \mathcal{N}(\mathcal{N}+1)$ with $\mathcal{N}$ an integer number specifying the last occupied shell) the $\Delta n_1 = 1$, $\Delta n_2 = -1$ ph transitions are Pauli-blocked thus completely inhibiting the ω_- mode. This excitation is switched on (with a sudden increase in strength) only when the deformation or B are high enough to break the closed shell structure, which takes place in first instance when

$$\frac{\omega_2}{\omega_1} = \frac{\mathcal{N}}{\mathcal{N}+1}\,. \quad (11)$$

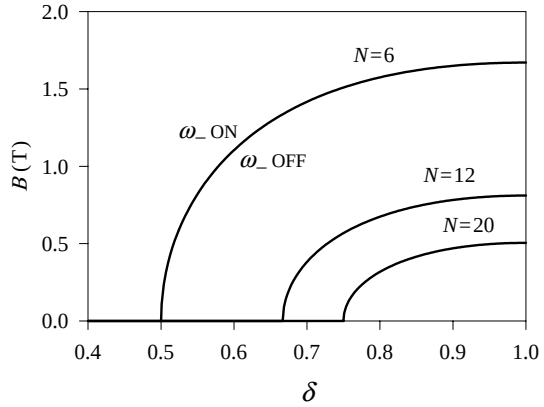

Fig. 2. The lines show the boundary between regions for ω_- mode in the NIDHO model and different dot sizes. Left and right of each curve correspond to ω_- being active or non-active (Pauli blocked) respectively. As in Figure 1 we have fixed $\omega_0(N=6)$ and used the jellium-disk relation $\omega_0(N_1)/\omega_0(N_2) = (N_2/N_1)^{1/4}$ for increasing sizes.

Figure 2 displays the regions in the (δ, B) plane in which the ω_- mode is active, for different dot sizes. This effect is absent for non-magic electron numbers since there is no Pauli blocking for these systems and, as a consequence, ω_- is active at all δ and B. For $N = 12, 20, \ldots$, subsequent changes in the ground state level structure give also rise to enhancements of the ω_- strength by allowing an increasing number of ph transitions. The mechanism discussed here is also responsible for strong enhancements of the moment of inertia in these systems [21].

The general situation in Figure 1 is qualitatively very similar for the deformations $\delta = 0.9$ and 0.7, we remark however that for $\delta = 0.7$ the *splitting* $\omega_{11} - \omega_{22}$ is higher at low B and the ω_- mode switches on at a smaller magnetic field. For large deformations ($\delta = 0.4$) the ω_- mode is active even at $B = 0$. Notice also that the splitting $\omega_{11} - \omega_{22}$ is so high that ω_{22} approaches ω_- at vanishing magnetic fields. A common feature to all deformations is that ω_{22} dominates the response at high B's. Altogether, the NIDHO model provides a quite interesting scenario of the M1 channel, with the emergence of novel modes and big strength transfers between them as a function of the magnetic field and deformation.

2.3 E2 response

The E2 strength is given in terms of the quadrupole operator xy by

$$S_{\rm E2}(\omega) = \sum_{hp} f_h(1-f_p)\ \left|\langle n_1^h n_2^h|U^{-1}xyU|n_1^p n_2^p\rangle\right|^2 \times\delta(E_p - E_h - \omega). \quad (12)$$

In a way similar to the M1 analysis we may obtain the E2 matrix elements. After a straightforward calculation one finds the same four modes of the M1 channel manifesting in the E2 spectra, although with different strengths (see third column in Fig. 1). The detailed expressions are

$$S_{\rm E2}(\omega_{11}) = \frac{\beta^2}{4}\sum_{\text{occ. levels}}(1-f_{n_1+2\,n_2})(n_1+1)(n_1+2)$$

$$S_{\rm E2}(\omega_{22}) = \frac{\beta^2}{4}\sum_{\text{occ. levels}}(1-f_{n_1\,n_2+2})(n_2+1)(n_2+2)$$

$$S_{\rm E2}(\omega_+) = \frac{(1-\beta^2 M_1 M_2\omega_1\omega_2)^2}{M_1 M_2\omega_1\omega_2} \times\sum_{\text{occ. levels}}(1-f_{n_1+1\,n_2+1})(n_1+1)(n_2+1)$$

$$S_{\rm E2}(\omega_-) = \frac{(1+\beta^2 M_1 M_2\omega_1\omega_2)^2}{M_1 M_2\omega_1\omega_2} \times\sum_{\text{occ. levels}}(1-f_{n_1+1\,n_2-1})(n_1+1)n_2. \quad (13)$$

We notice that the share of strength as a function of the magnetic field and deformation is similar to the magnetic dipole case. Several differences may, however, be remarked. Firstly, the ω_+ mode is relatively enhanced for all δ and B as compared to the results for the M1 channel. For instance the intensity ratio $I_{\rm E2}(\omega_+)/I_{\rm E2}(\omega_-)$ is enhanced by a factor ≈ 4 at $\delta = 0.4$ and $B = 0$. It is also worth to point out that the ω_{11} and ω_{22} intensities are reverted with respect to the M1 result. Finally, at large magnetic fields the low energy ω_{22} mode is no longer the dominant one since both ω_{11} and ω_- show a higher intensity.

As remarked above the number of electrons in Figure 1 ($N = 6$) corresponds at low deformations $\delta \to 1$ to a closed shell quantum dot. When analysing the M1 and E2 responses of dots that correspond to open shells in the circular limit the results are quite similar to those in this Figure, but with the important difference that the ω_- mode is already active at $B = 0$ since Pauli blocking is not effective in this case.

3 Role of the interaction

3.1 The method

To analyze the role of electron-electron interactions in a microscopic formalism we resort to the LSDA version of density functional theory. Besides the electron-electron repulsion contained in the selfconsistent electrostatic potential, the LSDA includes electronic exchange and correlation effects by relying on exact calculations for the uniform electron gas. At different levels, density functional theory has been applied by many authors to describe the ground state [27–31] and excitations of quantum dots [7–9,32]. The most refined version is the so-called current-density functional, first applied to quantum dots by Ferconi and Vignale [27], that was recently used to describe the edge reconstruction in these systems for large magnetic fields [33]. Nevertheless, current terms are known to be rather small for moderate magnetic fields and will be neglected in this work in which we shall resort to the approach of reference [8], developed for the

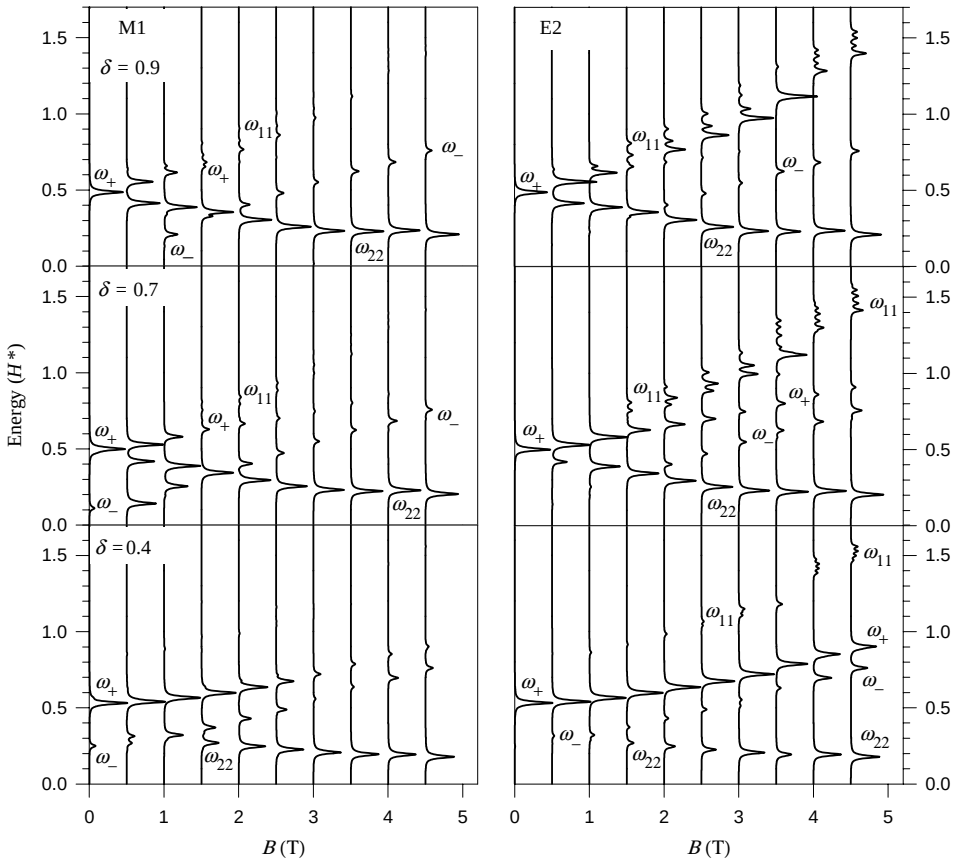

Fig. 3. M1 an E2 absorption intensities within LSDA for different magnetic fields and deformations. The results correspond to the same dot of Figure 1.

treatment of noncircular nanostructures. The importance of exchange and correlation on the M1 and E2 response functions will be quantified by comparing the LSDA with the results of the Hartree model, which totally neglects exchange and correlation.

The description of excitations in deformed nanostructures constitutes a highly nontrivial task, mainly because of the lack of symmetry not allowing the analytic integration of angular variables as in circular systems. For this reason we shall use the time-dependent LSDA to obtain the time evolution, following an initial perturbation, of relevant expectation values. The set of single-particle orbitals $\{\varphi_i(\mathbf{r})\}$ evolves in time as

$$\mathrm{i}\frac{\partial}{\partial t}\varphi_{i\eta}(\mathbf{r},t) = h_\eta[\rho,m]\,\varphi_{i\eta}(\mathbf{r},t)\ , \tag{14}$$

where $\eta = \uparrow,\downarrow$ is the spin index, and total density and magnetization are given in terms of the spin densities $\rho_\eta(\mathbf{r}) = \sum_i |\varphi_{i\eta}(\mathbf{r})|^2$, by $\rho = \rho_\uparrow + \rho_\downarrow$ and $m = \rho_\uparrow - \rho_\downarrow$, respectively. The Hamiltonian h_η in equation (14) contains, besides of kinetic energy, the confining $v^{(\mathrm{conf})}(\mathbf{r})$ potential and the selfconsistent Hartree

$$v^{(H)}(\mathbf{r}) = \int \mathrm{d}\mathbf{r}'\,\frac{\rho(\mathbf{r}')}{|\mathbf{r}-\mathbf{r}'|} \tag{15}$$

and exchange-correlation

$$v_\eta^{(xc)}(\mathbf{r}) = \frac{\partial}{\partial\rho_\eta}\mathcal{E}_{xc}(\rho,m) \tag{16}$$

contributions. In the Hartree model we neglect $v_\eta^{(xc)}$. The exchange-correlation energy density $\mathcal{E}_{xc}$ has been described as in references [7–9,32].

An initial perturbation of the orbitals $\varphi'(\mathbf{r}) = \mathcal{P}\varphi(\mathbf{r})$ models the interaction with the external field. The unitary operator $\mathcal{P}$ is given in terms of a displacement field $\mathbf{u}(\mathbf{r})$ as

$$\mathcal{P} = \exp\left[\mathrm{i}\mathbf{u}(\mathbf{r})\cdot\mathbf{p}\right]. \tag{17}$$

The appropriate fields for the M1 and E2 channels are $\mathbf{u}_{\mathrm{M1}} = \lambda r\,\mathbf{e}_\theta$ and $\mathbf{u}_{\mathrm{E2}} = \lambda\nabla(xy)$, where λ is a small parameter that guarantees the linear regime. Actually, these operators correspond to a rigid rotation (M1) and a quadrupole distortion (E2) of the electronic orbitals. After the initial distortion we keep track of $\langle\sum_i \ell_z^{(i)}\rangle(t)$ or $\langle\sum_i x_i y_i\rangle(t)$ and a subsequent frequency analysis of the signal provides the absorption energies and their associated strengths [8,20].

3.2 LSDA results and discussion

Figure 3 summarizes the M1 and E2 spectra of the $N = 6$ electron dot within time-dependent LSDA. Quite remarkably many features of the NIDHO model are also

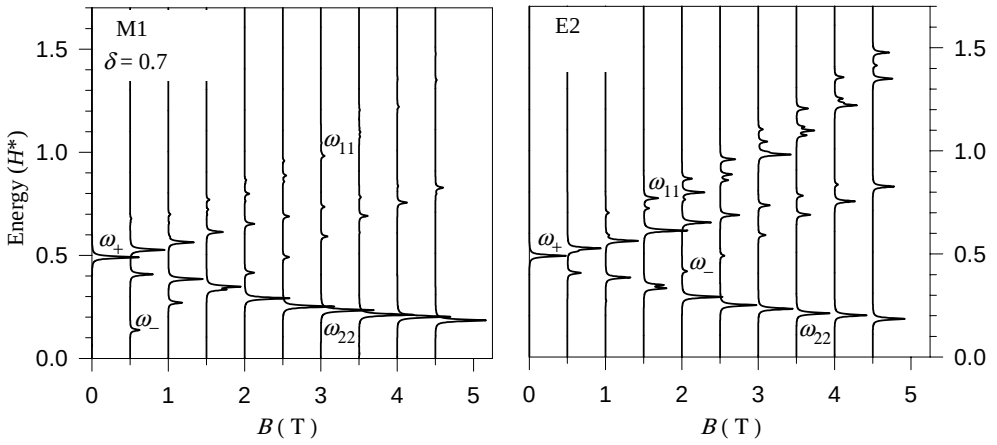

Fig. 4. Same as Figure 3 within the Hartree approximation for the intermediate deformation.

present in the LSDA spectra. In fact we can identify the four modes, labeled in Figure 3 by analogy with the NIDHO results, although in general they lie at different energies because of the interactions.

Focusing on the M1 channel, we notice for $\delta = 0.9$ the emergence of the low energy mode ω_- and its crossing with the ω_{22} mode. This crossing takes place at $B \approx 1.5$ T for both $\delta = 0.9$ and $\delta = 0.7$ and at $B \approx 1$ T for $\delta = 0.4$. The dominance of ω_{22} at large B's is also in very good agreement with the NIDHO prediction. We also remark that for $\delta = 0.7$ the ω_- mode is switched on even at $B = 0$ as a result of the interactions. At $\delta = 0.4$ the closeness of ω_{22} and ω_- at low magnetic fields predicted in the non-interacting case is nicely seen in Figure 3. It is also worth to mention the strong quenching of the ω_{11} mode within LSDA.

The E2 results also reflect to a great extent the systematics predicted by the NIDHO model. In general the high energy modes ω_+ and ω_{11} are more important in the E2 spectra than in the M1 ones, especially at large magnetic fields. In some cases the LSDA strengths show some small fragmentations that we attribute to ph effects (Landau damping). For instance, this is quite clear in the ω_{11} mode at 3 and 4 teslas.

3.3 Hartree results

The basic trends discussed in the preceding subsection are not significantly modified if the exchange and correlation contributions to equation (14) are neglected, *i.e.*, if one resorts to the Hartree model. Figure 4 shows the corresponding M1 and E2 absorption intensities for a deformation of $\delta = 0.7$. The results look very similar to the intermediate panels of Figure 3 thus indicating that the exchange and correlation do not play a relevant role in the formation of these collective modes. Nevertheless, some differences can be noted, as the higher relative strength of the ω_-(M1) for $B < 2$ T in LSDA and the different fragmentation of the high energy mode ω_{11}(E2) in the LSDA and Hartree models.

4 Summary and conclusions

The M1 and E2 channels of elliptic quantum dots are characterized by four modes whose energies and strengths vary with magnetic field and deformation. Their main characteristics are already seen in a non-interacting model, although interactions shift the mode energies and introduce several minor differences. The comparison of LSDA and Hartree results indicates that exchange and correlation effects are not very important in the characterization of the M1 and E2 responses. The main trends seen in Figures 1–4 may be summarized as follows:

a) Three modes ω_{11}, ω_+ and ω_- have a positive dispersion relation with B while the other ω_{22} exhibits a negative one. At low magnetic fields and deformations ω_{11}, ω_+ and ω_{22} are very close, while ω_- lies at a much lower energy. As the deformation is increased the three upper modes separate in energy (at $B \approx 0$), the lower of them ω_{22} coming close to ω_-.
b) At low B's the M1 strength of closed shell dots is exhausted by ω_+ while, when increasing the deformation ω_- becomes also active. This mode is also switched on when increasing the magnetic field for a fixed deformation as a consequence of the Pauli blocking mechanism. Generally, a crossing between ω_- and ω_{22} occurs for intermediate magnetic fields. At large magnetic fields the low energy ω_{22} mode eventually takes all the strength.
c) The E2 spectra are similar to the M1 ones, although an important amount of strength shifts to the high energy modes ω_+, ω_- and ω_{11} as compared to the magnetic dipole channel. Contrary to the M1 case the E2 absorption does not show a clear dominant peak at high B's.

This work was supported by Grant No. PB98-0124 from DGESeIC, Spain.

References

1. Ch. Sikorski, U. Merkt, Phys. Rev. Lett. **62**, 2164 (1989)
2. T. Demel, D. Heitmann, P. Grambow, K. Ploog, Phys. Rev. Lett. **64**, 788 (1990)
3. L. Brey, N.F. Johnson, B.I. Halperin, Phys. Rev. B **40**, 10647 (1993)
4. P.A. Maksym, T. Chakraborty, Phys. Rev. Lett. **65**, 108 (1990)
5. D.A. Broido, K. Kempa, P. Bahshi, Phys. Rev. B **42**, 11400 (1990)
6. V. Gudmundsson, R.R. Gerhardts, Phys. Rev. B **43**, 12098 (1991)
7. Ll. Serra, M. Barranco, A. Emperador, M. Pi, E. Lipparini, Phys. Rev. B **59**, 15290 (1999)
8. A. Puente, Ll. Serra, Phys. Rev. Lett. **83**, 3266 (1999)
9. C.A. Ullrich, G. Vignale, Phys. Rev. B **61**, 2729 (2000)
10. I. Magnusdottir, V. Gudmundsson, Phys. Rev. B **60**, 16591 (1999)
11. B.P. van Zyl, E. Zaremba, D.A.W. Hutchinson, Phys. Rev. B **61**, 2107 (2000)
12. R. Strenz, U. Bockelmann, F. Hirler, G. Abstreiter, G. Böhm, G. Weimann, Phys. Rev. Lett. **73**, 3022 (1994)
13. D.J. Lockwood, P. Hawrylak, P.D. Wang, C.M. Sotomayor Torres, A. Pinczuk, B.S. Dennis, Phys. Rev. Lett. **77**, 354 (1996)
14. C. Schüller, G. Biese, K. Keller, C. Steinebach, D. Heitmann, P. Grambow, K. Eberl, Phys. Rev. B **54**, 17304 (1996)
15. C. Schüller, K. Keller, G. Biese, E. Ulrichs, L. Rolf, C. Steinebach, D. Heitmann, K. Eberl, Phys. Rev. Lett. **80**, 2673 (1998)
16. C. Steinebach, C. Schüller, D. Heitmann, Phys. Rev. B **59**, 10240 (1999)
17. O. Steffens, M. Suhrke, Phys. Rev. Lett. **82**, 3891 (1999)
18. M. Barranco, L. Colletti, E. Lipparini, A. Emperador, M. Pi, Ll. Serra, Phys. Rev. B **61**, 8289 (2000)
19. D.G. Austing, S. Sasaki, S. Tarucha, S.M. Reimann, M. Koskinen, M. Manninen, Phys. Rev. B **60**, 11514 (1999)
20. Ll. Serra, A. Puente, E. Lipparini, Phys. Rev. B **60**, 13966 (1999)
21. Ll. Serra, A. Puente, E. Lipparini, Physica E (2002), in press (available online, DOI: 10.1016/S1386-9477(01)00238-7)
22. Unless stated otherwise, we shall use effective atomic units for which $\hbar^2 = e^2/\kappa = m = 1$, with κ and m the dielectric constant and electron effective mas, respectively Assuming GaAs values one has $H^* \approx 12$ meV, $a_0^* \approx 98$ Å and $\tau^* \approx 55$ fs, as energy, length and time units
23. For bulk GaAs the effective gyromagnetic factor is $g^* = -0.44$. As usual it is also defined $m^* = m/m_e$, the dimensionless effective mass constant, which for GaAs is 0.067
24. O. Dippel, P. Schmelcher, L.S. Cederbaum, Phys. Rev. A **49**, 4415 (1994)
25. A.V. Madhav, T. Chakraborty, Phys. Rev. B **49**, 8163 (1994)
26. J.J. Sakurai, *Modern Quantum Mechanics* (Addison-Wesley, Reading 1994), p. 96
27. M. Ferconi, G. Vignale, Phys. Rev. B **50**, 14722 (1994)
28. O. Heinonen, M.I. Lubin, M.D. Johnson, Phys. Rev. B **56**, 10373 (1997)
29. M. Koskinen, M. Manninen, S.M. Reimann, Phys. Rev. Lett. **79** 1389 (1997)
30. M. Pi, M. Barranco, A. Emperador, E. Lipparini, Ll. Serra, Phys. Rev. B **57**, 14783 (1998)
31. K. Hirose, N.S. Wingreen, Phys. Rev. B **59**, 4604 (1999)
32. E. Lipparini, M. Barranco, A. Emperador, M. Pi, Ll. Serra, Phys. Rev. B **60**, 8734 (1999)
33. S.M. Reimann, M. Koskinen, M. Manninen, B.R. Mottelson, Phys. Rev. Lett. **83**, 3270 (1999)